# Adsorption of Remazol Brilliant Blue R using ZnO fine powder: Equilibrium, kinetic and thermodynamic modeling studies

Kezban Ada [a], Aysun Ergene [b,*], Sema Tan [b], Emine Yalçın [b]

[a] Department of Chemistry, Faculty of Arts and Sciences, Kırıkkale University, 71450 Yahşihan-Kırıkkale, Turkey
[b] Department of Biology, Faculty of Arts and Sciences, Kırıkkale University, 71450 Yahşihan-Kırıkkale, Turkey

## ABSTRACT

Zinc oxide powders with six-sided flake-like particles were prepared by homogeneous precipitation from boiling aqueous solutions that contained excess urea and 0.075 (Z075) and 0.300 (Z300) M $Zn^{2+}$. The average sizes of the particles are 37 and 46 $\mu$m, while the average sizes of the crystals are ~45 for Z075 and Z300 at 1000 °C. Equilibrium, kinetic and thermodynamic studies were carried out for the adsorption of RBBR dye from aqueous solution using both types of ZnO in the form of fine powders. The effects of pH, initial dye concentration, contact time and temperature of solution on the adsorption were studied. Langmuir, Temkin and Dubinin–Radushkevich (D–R) isotherm models were used to describe the adsorption of RBBR onto ZnO powders. The Langmuir and D–R isotherm models fit the equilibrium data better than the Temkin isotherm model. The monomolecular adsorption capacity of Z075 and Z300 was determined to be 190 and 345 mg g$^{-1}$ for RBBR, respectively. The Lagergren first-order, Ritchie second-order kinetic and intra-particle diffusion models were used for the adsorption of the dye onto ZnO powders. The Ritchie second-order model was suitable for describing the adsorption kinetics for the removal of RBBR from aqueous solution onto Z075 and Z300. Thermodynamic parameters, such as the Gibbs free energy ($\Delta G^{\#}$), enthalpy ($\Delta H^{\#}$), entropy ($\Delta S^{\#}$) and equilibrium constant of activation ($K^{\#}$) were calculated. These parameters showed that the adsorption process of RBBR onto Z075 and Z300 was an endothermic process of a chemical nature under the studied conditions.

© 2008 Elsevier B.V. All rights reserved.

## 1. Introduction

Zinc oxide (ZnO) powders have potential applications in various fields, such as varistors (variable resistor), transducers, semiconductors, solar cells, non-linear optical materials, gas sensors, ceramics, pigments, rubber additives, photo-catalysts, rubber additives, pharmaceuticals, cosmetics and so on [1–5]. A wide number of methods have been used to prepare ZnO powders, including, homogeneous precipitation in aqueous solution of $Zn^{2+}$ cations, hydrothermal synthesis, microwave synthesis, solution combustion, pulsed laser deposition, emulsion precipitation, ultrasonic atomization, spray pyrolysis, freeze-drying and sol–gel processes [6–15].

The microstructural and morphological characteristics of ZnO powders vary according to the selected synthesis method. ZnO powders of different shapes, such as spindle-like, rod-like, ellipsoidal, spherical, and prismatic have been synthesized by the one

or more of the methods mentioned above [16–22]. On the other hand, only a few methods were reported in the literature [23] to prepare ZnO powder having flake-like particles. The aim of this study is the chemical preparation of flake-like ZnO particles using a reaction between zinc sulfate and excess urea in a boiling aqueous solution.

Synthetic dyes are extensively used for textile dyeing and other industrial applications. The total world colorant production is estimated to be about 800,000 tons/year. More than 10,000 dyes are commercially available and at least 10% of the used dyestuff enters the environment as wastes [24]. These industrial effluents are toxic and are characterized by high chemical oxygen demands (CODs)/biological oxygen demands (BODs), suspended solids and intense color [25]. Furthermore, these colored molecules are highly conjugated and can be extremely injurious to the life forms [26]. Synthetic dyes, classified by their chromophores, have different and stable chemical structures to meet various coloring requirements and they are often difficult to degrade and/or removed by conventional physical and chemical processes [27,28].

Remazol Brilliant Blue R dye (RBBR) is one of the most important dyes in the textile industry. It is frequently used as a starting

* Corresponding author. Tel.: +90 318 3572478/1518; fax: +90 318 3572461.
E-mail address: ayergene@yahoo.com (A. Ergene).

material in the production of polymeric dyes. RBBR is an anthracene derivative and represents an important class of toxic and recalcitrant organopollutants.

## 2. Materials and methods

### 2.1. Preparation of ZnO fine powders

The preparation and some physicochemical properties of the ZnO powders selected as materials in this study were investigated in our previous work [29]. The zinc oxide precursors were precipitated in boiling aqueous solution containing 0.075 and 0.300 M $Zn^{+2}$ and excess urea. The powders were obtained by the calcination of the precursors at 1000 °C for 4 h. The powders that were prepared at two different concentrations are called, for the purposes of this study Z075 and Z300. Scanning electron microscopy (SEM) photographs for Z075 and Z300 were recorded (LEO 435) at 30 kV from samples covered with a gold thin film.

### 2.2. Preparation of dye

The general characteristics of RBBR are summarized in Table 1. RBBR (CI 61200, Reactive Blue 19) obtained from Sigma–Aldrich Company Ltd, is an anthraquinone-based dye. The concentration of the prepared dye solutions ranged between 0.5 and 10 g L$^{-1}$ for RBBR.

### 2.3. Adsorption isotherms in a batch system

The three most common adsorption isotherm models were used to fit the equilibrium adsorption data. These are the Langmuir, Temkin and Dubinin–Radushkevich models. The linear form of the Langmuir equation [30–33], is expressed by

$$\frac{C_e}{q_e} = \frac{1}{q_m}K_L + \frac{C_e}{q_m} \tag{1}$$

where $K_L$ denotes the Langmuir isotherm constant related to the affinity between the adsorbent and the adsorbate (L g$^{-1}$) and $q_m$ denotes the Langmuir monomolecular adsorption capacity (mg g$^{-1}$). The values of $q_m$ and $K_L$ can be determined by plotting $C_e/q_e$ versus $C_e$. Equation of the Temkin model [34–36] is given below and is plotted as $q_e$ against $\ln C_e$:

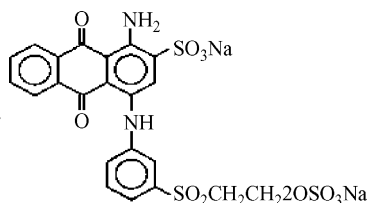$$q_e = \left(\frac{RT}{b_T}\right)\ln K_T + \left(\frac{RT}{b_T}\right)\ln C_e \tag{2}$$

where $b_T$ is the adsorption potential of the adsorbent and $K_T$ is the equilibrium constant corresponding to maximum binding energy (L g$^{-1}$). $K_T$ and $\Delta G^\circ$ as follows:

$$K_T = \exp\left(\frac{-\Delta G^\circ}{RT}\right) \tag{3}$$

where $R$ is the universal constant and $T$ is the absolute temperature.

**Table 1**

The characteristics of RBBR.



| | |
|---|---|
| Molecular formula | $C_{22}H_{16}N_2Na_2O_{11}S_3$ |
| Molecular weight | 626.54 |
| Color index number | 61,200 |
| $\lambda_{max}$ (nm) | 595 |

The linear form of the Dubinin–Radushkevich model [34–37] is represented by equation:

$$\ln q_e = \ln q_m - K_{DR}\varepsilon^2 \tag{4}$$

where $K_{DR}$ is the porosity factor (mol$^2$ J$^{-2}$), $q_m$ (mol g$^{-1}$) is the monomolecular adsorption capacity of adsorbate adsorption by the powder surface and the variable $\varepsilon$ can be related to equilibrium concentration ($C_e$, g L$^{-1}$) as follows:

$$\varepsilon = RT\ln\left[1 + \frac{1}{C_e}\right] \tag{5}$$

where $\varepsilon$ (J mol$^{-1}$) is the Polonyi potential, $R$ is the universal gas constant and equal to 8.314 J mol$^{-1}$ K$^{-1}$ and $T$ is the absolute temperature.

A plot of $\ln q_e$ versus $\varepsilon^2$ (J$^2$ mol$^{-2}$) yields a straight line, confirming the model. The mean free energy of adsorption $E$ (kJ mol$^{-1}$) per molecule of the adsorbate when it is transferred from the solution to the powder surface can be calculated using the following equation:

$$E = (-2K_{DR})^{-1/2} \tag{6}$$

### 2.4. Kinetic models for the adsorption

To determine dye adsorption kinetics, three different kinds of kinetic models were used. The Lagergren pseudo-first-order, pseudo-second-order and intra-particle diffusion kinetic models are shown below [33,34,38–41].

The pseudo-first order model is defined by the equation:

$$\frac{dq_t}{dt} = k_1(q_e - q_t) \tag{7}$$

where $t$ is the contact time (min), $k_1$ is the pseudo-first-order adsorption rate constant (min$^{-1}$), $q_e$ and $q_t$ are the amount of dye adsorbed on the ZnO fine powders at equilibrium (mg g$^{-1}$) and at time $t$, respectively. The integration of Eq. (7) with the initial condition, $q_t = 0$ at $t = 0$ leads to:

$$\ln(q_e - q_t) = \ln q_e - k_1 t \tag{8}$$

The values of the adsorption rate constant ($k_1$) were determined from the $\ln(q_e - q_t)$ in terms of $t$.

The pseudo-second-order model is defined by

$$\frac{dq_t}{dt} = k_2(q_e - q_t)^2 \tag{9}$$

Integrating and rearranging Eq. (9) with the initial condition $q_t = 0$ at $t = 0$, the following equation is obtained:

$$\frac{t}{q_t} = \frac{1}{h} + \left(\frac{1}{q_e}\right)t \tag{10}$$

where $dq_t/dt$ is the initial sorption rate (mg g$^{-1}$ min$^{-1}$) and is defined as $t \to 0$ by $H = k_2 q_e^2$ where $k_2$ is the pseudo-second-order adsorption rate constant (g mg$^{-1}$ min$^{-1}$). The value $q_e$ is determined from the slope of $t/q_t$ versus $t$ and $h$ is determined from the intercept.

*Intra-particle diffusion model*: The adsorption of RBBR dye onto ZnO fine powders may be controlled via external film diffusion at earlier stages and later by the particle diffusion. The possibility of intra-particle diffusion resistance was identified by using the following intra-particle diffusion model:

$$q_t = K_{dif}t^{1/2} + C \tag{11}$$

where $K_{dif}$ is the intra-particle diffusion rate constant (mg g$^{-1}$ min$^{-1/2}$) and $C$ is the intercept. The values of $q_t$ versus $t^{1/2}$ and the rate constant $K_{dif}$ are directly evaluated from the slope of the regression line.

## 2.5. Determination of the activation energy and frequency factor

The rate constant ($k$) were determined from Eq. (10) at different temperatures and were used to estimated the activation energy of RBBR onto Z075 and Z300. The rate constant is expressed as a function of temperature according to the well known Arrhenius equation:

$$\ln k = \frac{\ln A - E^{\#}}{RT} \tag{12}$$

where $E^{\#}$ (kJ mol$^{-1}$) is the activation energy of adsorption, $A$ (g mol$^{-1}$ s$^{-1}$) is the temperature-independent frequency factor, $R$ (8.314 J mol$^{-1}$ K$^{-1}$) is the universal gas constant and $T$ (K) is the absolute temperature.

## 2.6. Thermodynamics of the adsorption

The relation between rate constant ($k$) and equilibrium constant ($K^{\#}$) can be given in the form [29,41]:

$$k = \left(\frac{k_B T}{h}\right) K^{\#} \tag{13}$$

where $k_B = 1.381 \times 10^{-23}$ J K$^{-1}$ is the Boltzmann constant, $h = 6.626 \times 10^{-34}$ J s is the Planck constant, and $T$ is the absolute temperature. The value of $K^{\#}$, was calculated from this relation ($K^{\#} = 4.80 \times 10^{-11}$ k/T) for each temperature.

The relation between the activation energy and internal energy of activation ($\Delta U^{\#}$) can be derived by using the well-known Arrhenius ($d \ln k/dT = E^{\#}/RT^2$) and van't Hoff ($d \ln K^{\#}/dT = \Delta U^{\#}/RT^2$) equations in the temperature derivative of the last equation as follows:

$$d \ln \frac{k}{dT} = \left(\frac{1}{T}\right) + d \ln \frac{K^{\#}}{dT} \tag{14}$$

$$\frac{E^{\#}}{RT^2} = \left(\frac{1}{T}\right) + \frac{\Delta U^{\#}}{RT^2} \tag{15}$$

$$\Delta U^{\#} = E^{\#} - RT \tag{16}$$

The relation between the enthalpy ($\Delta H^{\#}$) and internal energy of activation ($\Delta U^{\#}$) can be given in the form:

$$\Delta H^{\#} = \Delta U^{\#} + \Delta \nu^{\#} RT = E^{\#} - RT + (1 - m)RT = E - mRT \tag{17}$$

where $\Delta H^{\#}$ is enthalpy of activation, $\Delta \nu^{\#} = 1 - m$ is the stoichiometric value of the activation reaction and $m$ is the molecularity, which is equal to the order.

The $\Delta H^{\#}$ value for each temperature was calculated from the last equation. The Gibbs free energy for activation ($\Delta G^{\#}$) and entropy of activation ($\Delta S^{\#}$) were calculated from the equation:

$$\Delta G^{\#} = \Delta H^{\#} - T \Delta S^{\#} = - RT \ln K^{\#} \tag{18}$$

## 2.7. Adsorption studies

In order to obtain isotherm and kinetic data, ZnO powders were performed in 100 mL Erlenmeyer flasks containing 20 mL synthetic dye solutions. The flasks were agitated on a shaker at 150 rpm for 24 h to ensure that equilibrium was reached.

The effect of the initial pH on the adsorption capacity of the Z075 and Z300 was investigated in the pH range of 2.0–8.0 (which was adjusted with HCl or NaOH solution at the beginning of the experiment) at 25 °C. The effect of temperature was studied at three different temperatures (15, 25 and 40 °C) at pH 4.0. The effect of initial dye concentration between 50 and 1000 ppm on the decolorization capacities of the powders was studied.

The amount of adsorbed dye per unit ZnO fine powder (mg dye/g ZnO) was determined by using the following equation:

$$q_e = (C_0 - C_e)\frac{V}{m} \tag{19}$$

where $q_e$ is the adsorption capacity (mg g$^{-1}$) and $C_0$ and $C_e$ are the concentration of the dye in the solution (mg L$^{-1}$) before and after adsorption, respectively. $V$ is the volume in aqueous solution (L) and $m$ is the ZnO weight (g).

## 2.8. Analysis of RBBR

The concentration of the unadsorbed RBBR dye in the biosorption medium was measured colorimetrically using a spectrophotometer (Spectro RS). The adsorbance of the color was read at 595 nm.

## 3. Results and discussion

### 3.1. Properties of prepared ZnO powders

The SEM photographs for ZnO powders were examined and representative photographs, for Z075 and Z300 are given in Fig. 1. As seen from the SEM view, the particles have the shape of well-formed hexagonal plates. Some physicochemical properties of the prepared ZnO powders are shown in Table 2 [29].

### 3.2. Effect of adsorbent concentration

As shown in Fig. 2, the amount of adsorbed RBBR onto the Z075 and Z300 at equilibrium were studied and plotted as a function of the initial concentration of the RBBR adsorption medium. The adsorption capacity, $q_e$ (mg g$^{-1}$), of Z075 and Z300 increased with
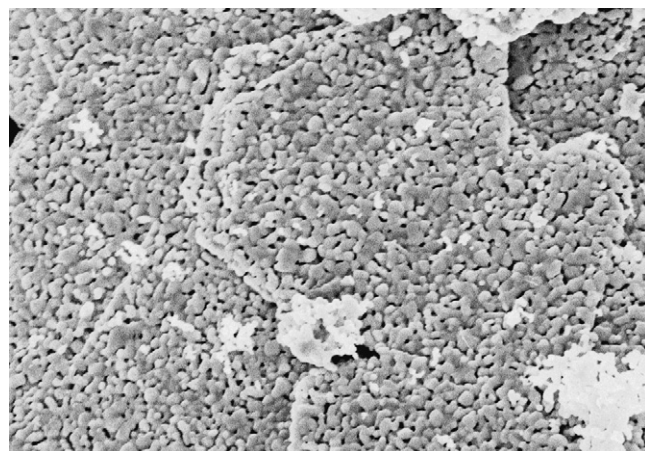


**Fig. 1.** The scanning electron microscope (SEM) photograph of the ZnO fine powder sample (Z075).

**Table 2**
Some physicochemical properties of the prepared ZnO powders ($D$: particle size, $L$: crystal size, $V$: specific micro-mesoporevolume, $S$: specific surface area, PSD: particle size distribution, SEM: scanning electron microscope, XRD: X-ray diffraction, N$_2$-AD: nitrogen adsorption, N$_2$-DE: nitrogen desorption).

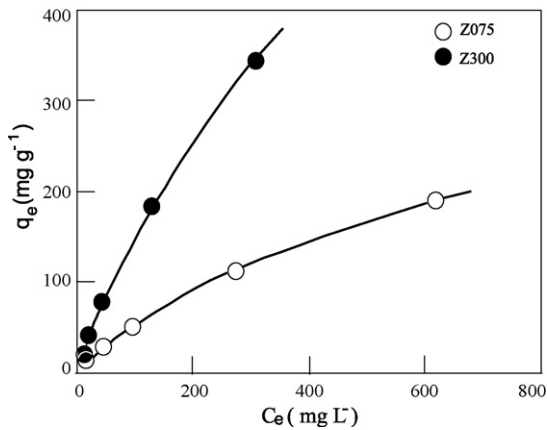| Properties | Methods | Samples | |
|---|---|---|---|
| | | Z075 | Z300 |
| $D_{pow}$ (μm) | SEM | 37 | 46 |
| $L_{pow}$ (nm) | XRD | 46 | 45 |
| $V_{pow}$ (cm$^3$ g$^{-1}$) | N$_2$-DE | 0.007 | 0.030 |
| $S_{pow}$ (m$^2$ g$^{-1}$) | N$_2$-AD | 1.9 | 0.4 |

Fig. 2. The adsorption capacity of Z075 and Z300 of the dye concentration at equilibrium for RBBR (pH 4.0, $t = 30\,°C$, agitation rate = 150 rpm).

increasing concentration of RBBR at equilibrium ($C_e$, mg L$^{-1}$). The monomolecular adsorption capacities of Z075 and Z300 are 190 and 345 mg g$^{-1}$ at 1000 ppm RBBR initial concentration, respectively. With the increasing concentration of adsorbent, the monomolecular adsorption capacity of the adsorbate increased.

### 3.3. Effect of initial pH on dye adsorption

The effects of initial pH on dye adsorption of Z075 and Z300 were studied in the pH range from 2.0 to 8.0 at an initial dye concentration of 1000 ppm and results are shown in Fig. 3. The maximum adsorption capacities of RBBR onto Z075 and Z300 were determined at pH 4.0 as 190 and 250 mg g$^{-1}$, respectively. The adsorption capacity increased from pH 5.0 to 7.0 after pH 7.0 the adsorption capacity decreased.

The pH of the dye solution plays an important role in the whole adsorption process. Many oxide surfaces create a surface charge (positive or negative) [42]. Dye adsorption is highly pH dependent. The anthraquinonic RBBR release colored dye anions in solution. The pH of the solution affects the surface charge of the adsorbent as well as the degree of ionization of the materials in the solution. Therefore, the pH affects the structural stability and color intensity of RBBR. X-ray studies [43] show that zinc oxide formed at 1000 °C has a complete crystallographic form that does not contain hydroxyl groups. Calcinated ZnO has hydroxyl groups only in acidic
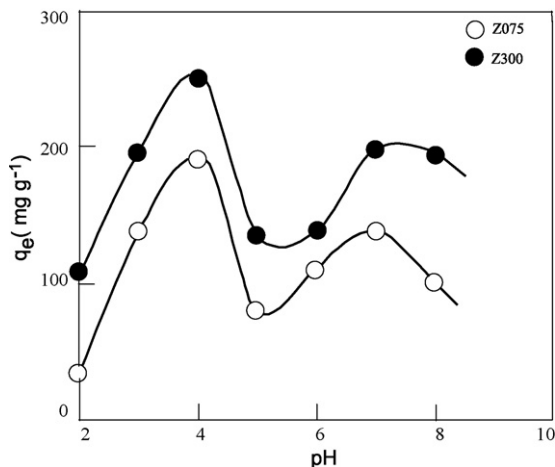


Fig. 3. The effect of initial pH on the equilibrium RBBR sorption capacity of Z075 and Z300 ($C_0 = 1000$ ppm, $t = 30\,°C$, agitation rate = 150 rpm).
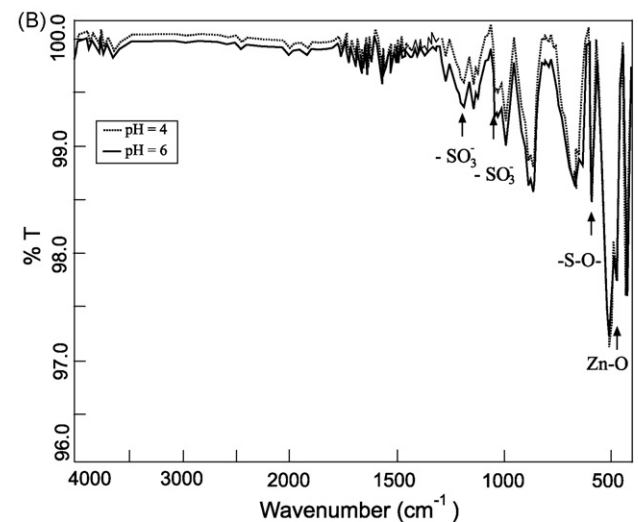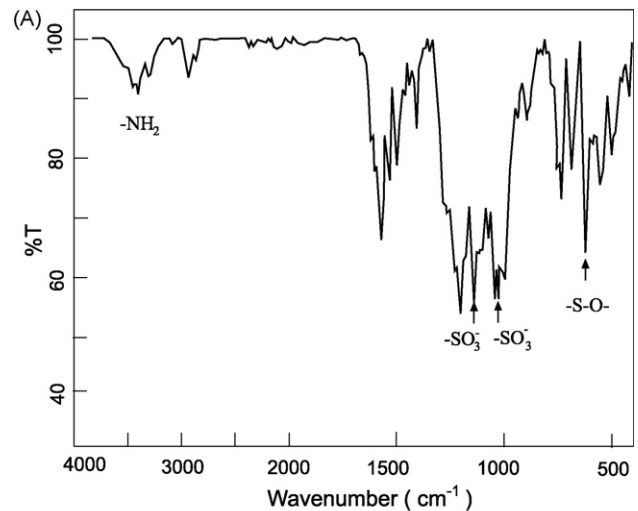




Fig. 4. (A) Transmission FT-IR spectra of RBBR dye. (B) Transmission FT-IR spectra of RBBR dye adsorbed onto ZnO.

solutions (pH 4.0 and 6.0) and is converted into an anion-exchanger [44].

Because of this, the adsorption must be due to the interaction of sulfonic ($-SO_3^-$) groups of dyes with $-OH$ groups on the surface of the fine ZnO powders [46]. The FT-IR spectra of RBBR dye and dye adsorbed ZnO powders are shown in Fig. 4A and B. As seen in Fig. 4A, the adsorption bands at 3295, 1200 and 1041 cm$^{-1}$ correspond to the $-NH_2-$ stretching vibration and asymmetric and symmetric $-S=O-$ stretching vibration from sulfonic ($-SO_3^-$) groups, respectively [46]. The peak intensities of the 1041, 1075 cm$^{-1}$ symmetric ($-SO_3^-$) and the 1137, 1201 cm$^{-1}$ symmetric ($-SO_3^-$) stretching vibrations are much higher at pH 6.0 than that at pH 4.0 [47]. The Zn–O (477, 513 cm$^{-1}$) adsorption bands are clearly delineated [48] (Fig. 4B). This indicates that more RBBR dye adsorbed onto ZnO powder at pH 4.0 [49].

### 3.4. Adsorption isotherms

Three important isotherm models were chosen to fit the experimental equilibrium data in this study. Adsorption isotherm model constants the values of which express the surface properties and affinity of the biosorbent can be used to compare the adsorption capacities of ZnO for RBBR dye. The isotherm constants are summa-

**Table 3**
Langmuir, Temkin and Dubinin–Radushkevich parameters for the adsorption isotherms of RBBR onto Z075 and Z300 (pH 4.0, $t = 25\,°C$, $V = 100\,mL$, $m = 0.2\,g\,L^-$).

| Isotherms | Powder | Constants | | $R^2$ |
|---|---|---|---|---|
| Langmuir | | $q_m$ (mg g$^{-1}$) | $K_L$ (L g$^{-1}$) | |
| $C_e/q_e = 1/q_m K_L + C_e/q_m$ | Z075 | 38.9 | 1.52 | 0.9981 |
| | Z300 | 89.3 | 2.01 | 0.9960 |

| Isotherms | Powder | Constants | | $R^2$ |
|---|---|---|---|---|
| Temkin | | $K_T$ (L mol$^{-1}$) | $\Delta G°$ (kJ mol$^{-1}$) | |
| $q_e = (RT/b_T)\ln K_T + (RT/b_T)\ln C_e$ | Z075 | 33.8 | −8.729 | 0.8725 |
| | Z300 | 46.4 | −9.510 | 0.9075 |

| Isotherms | Powder | Constants | | | $R^2$ |
|---|---|---|---|---|---|
| Dubinin–Radushkevich | | $K_{DR}$ (mol$^2$ J$^{-2}$) | $q_m$ (mg g$^{-1}$) | $E$ (kJ mol$^{-1}$) | |
| $\ln q_e = \ln q_m - K_{DR}\varepsilon^2$ | Z075 | 0.0056 | 30.2 | −9.450 | 1.000 |
| | Z300 | 0.0017 | 46.1 | −17.20 | 1.000 |

rized in Table 3. Analysis of the $R^2$ values (Table 3) showed that the Langmuir and Dubinin–Radushkevich equations have more precise coefficients than the Temkin equation for modeling the RBBR dye adsorption onto Z075 and Z300. The Langmuir adsorption isotherm was preferred for the estimation of the monomolecular adsorption capacity $q_m$ corresponding to complete monolayer coverage on the powder surfaces. The values of $q_m$, $K_L$ and the coefficient of determination $R^2$ are given in Table 3. The monomolecular adsorption capacity, $q_m$, showed that Z300 (89.3 mg g$^{-1}$) had more mass capacity than Z075 (38.9 mg g$^{-1}$). The Langmuir isotherm provided an acceptable fit indicating a homogeneous and monomolecular adsorption mechanism.

The Temkin isotherm model predicts a uniform distribution of binding energies over the population of surface binding adsorption sites. The range and distribution of the binding energies should depend strongly on the density and distribution of functional groups both on the dye and adsorbent surfaces. The Temkin adsorption isotherm model was chosen to determine the adsorption potentials of the adsorbent for adsorbates. The Temkin adsorption potentials $K_T$ for Z075 and Z300 are 33.8 and 46.4 L mol$^{-1}$, respectively.

The values of the standard free enthalpy, $\Delta G°$, were calculated according to Eq. (3) for Z075 and Z300 (−8729 and −9510 J mol$^{-1}$, respectively) in Table 3. These results show that in the Temkin isotherm model, binding energy increased with increasing amount of adsorbed dye on the adsorbent surface.

The Dubinin–Radushkevich model used to determine the characteristic porosity and the apparent free energy of adsorption. The isotherm parameters $q_m$ and $K_{DR}$ are presented in Table 3. The monomolecular adsorption capacities $q_m$ for Z075 and Z300 were 30.2 and 46.1 mg g$^{-1}$, respectively. The porosity factors $K_{DR}$ for Z075 and Z300 were 0.0056 and 0.0017 mol$^2$ J$^{-2}$, respectively. The apparent free energies from the Dubinin–Radushkevich model for Z075 and Z300 were calculated to be in the range of 9450–17,200 J mol$^{-1}$. The mean free energy of adsorption gives information about the adsorption mechanism as a chemical ion-exchange. If the value of $E$ is between 8 and 16 kJ mol$^{-1}$ then the adsorption process follows by chemical ion-exchange and if $E < 8$ kJ mol$^{-1}$ the adsorption process is of a physical nature. These results indicate that the adsorption process of dye (with –SO$_3^-$ groups) onto ZnO may be carried out via a chemical anion-exchange mechanism.

### 3.5. Adsorption kinetic models

The effect of time on RBBR dye adsorption for Z075 and Z300 were investigated in a batch system. The equilibrium adsorption capacities of the RBBR for Z075 and Z300 versus time are shown
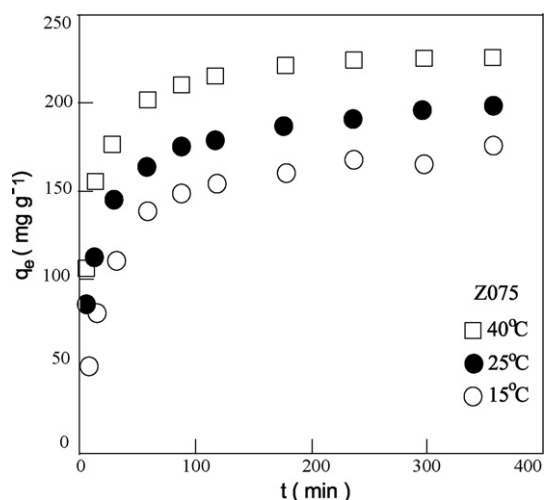


**Fig. 5.** The effect of contact time on the adsorption capacity of Z075 at different temperatures ($C_0$: 1000 ppm, pH: 4.0, agitation rate: 150 rpm).

in Figs. 5 and 6 at 15, 25 and 40 °C, respectively. Both Z075 and Z300 reached the saturation level in approximately 6 h. At the initial RBBR concentration (1000 ppm) in the batch system, the adsorption capacities were determined to be 210 and 285 mg g$^{-1}$
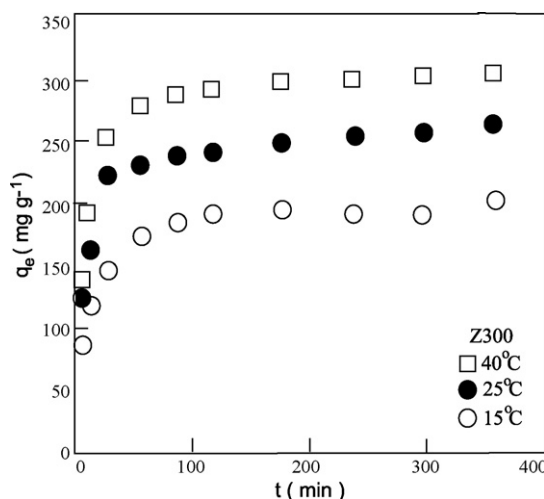


**Fig. 6.** The effect of contact time on the adsorption capacity of Z0300 at different temperatures ($C_0$: 1000 ppm, pH: 4.0, agitation rate: 150 rpm).

**Table 4**
Comparison of kinetic parameters of the Lagergren first-order, Ritchie second-order kinetic and intra-particle diffusion models for the removal of RBBR onto Z075 and Z300 ($C_0$ = 1000 ppm, 150 rpm, pH 4.0).

| | Experimental $q_{exp}$ (mg g$^{-1}$) | Lagergren first-order kinetic | | | Ritchie second-order kinetic | | | Intra-particle diffusion model | | |
|---|---|---|---|---|---|---|---|---|---|---|
| | | $k_1 \times 10^{-2}$ (min$^{-1}$) | $q_{eq}$ (mg g$^{-1}$) | $R^2$ | $k_2 \times 10^{-4}$ (g mg$^{-1}$ min$^{-1}$) | $q_{eq}$ (mg g$^{-1}$) | $R^2$ | $K_{dif}$ (mg g$^-$ min$^{-1/2}$) | $C$ | $R^2$ |
| **15 °C** | | | | | | | | | | |
| Z075 | 172.5 | 1.68 | 55.5 | 0.8408 | 3.25 | 175.4 | 0.9986 | 6.383 | 66.491 | 0.8150 |
| Z300 | 205.0 | 1.18 | 91.0 | 0.8517 | 6.72 | 196.1 | 0.9994 | 7.832 | 179.93 | 0.6777 |
| **25 °C** | | | | | | | | | | |
| Z075 | 195.0 | 2.14 | 77.5 | 0.9913 | 4.11 | 200.0 | 0.9995 | 5.842 | 100.05 | 0.8139 |
| Z300 | 257.5 | 2.38 | 110.7 | 0.9942 | 4.49 | 263.2 | 0.9995 | 6.379 | 154.16 | 0.7004 |
| **40 °C** | | | | | | | | | | |
| Z075 | 224.0 | 1.98 | 101.8 | 0.8512 | 5.83 | 227.3 | 1.0000 | 4.065 | 15891 | 0.7707 |
| Z300 | 300.0 | 2.39 | 126.3 | 0.9676 | 4.84 | 303.0 | 1.0000 | 5.383 | 107.74 | 0.6822 |

of RBBR adsorption onto Z075 and Z300 in 90 min, respectively. After 90 min, the adsorption capacity hardly changed during the adsorption time.

The experimental kinetic data of the adsorption studies were used in the Lagergren first-order, Ritchie second-order kinetic and intra-particle diffusion models. The first-order kinetic model indicates that the process of adsorption occurs at a rate proportional to dye concentration, which is suitable especially for low concentrations. The second-order kinetic model is derived from adsorption processes in which the rate-controlling step is an exchange reaction [39,40]. The rate constants $k$ and the intra-particle diffusion model constant $K_{dif}$ for the adsorption of the dye on the ZnO powder are presented in Table 4. The data obtained from the first-order kinetic equation were not well-defined for the adsorption of the tested dye on the powder.

As seen in Figs. 7 and 8, the experimental values of the maximum adsorption capacity $q_{exp}$ for Z075 and Z300 are very close to the calculated theoretical values $q_e$ of the second-order kinetic model. This process was suitable for the description of the adsorption kinetics for the removal of RBBR from aqueous solution onto Z075 and Z300. The adsorption can be seen as the rate-limiting step that controls the adsorption process.

As seen in Table 4, which shows the $K_{dif}$ values and coefficient constant, the intra-particle diffusion model cannot be the dominating mechanism for the adsorption of the RBBR from aqueous solution by the Z075 and Z300.
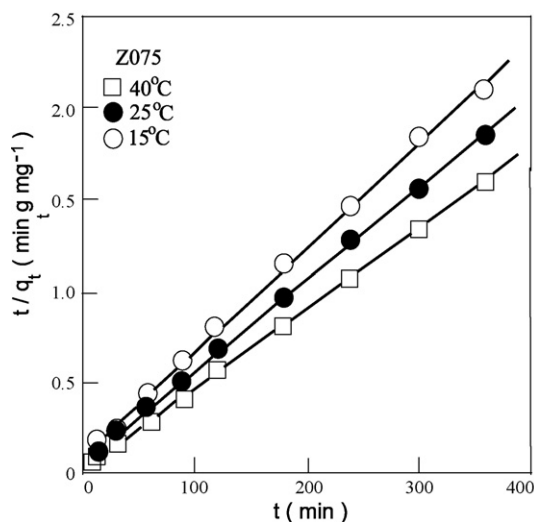


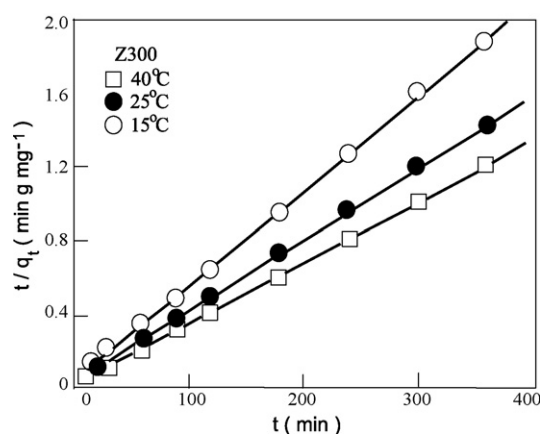**Fig. 8.** The second-order kinetic plots for adsorption of RBBR onto Z300.

### 3.6. Adsorption thermodynamics

According to the well-known Arrhenius equation, a plot of ln $k$ against $1/T$ is shown in Fig. 9. The activation energy, $E^\#$, and the frequency factor $A$ were calculated, respectively from the slope and the intercept of the straight line as seen in Fig. 9. By using these parameters, the temperature dependence of the adsorption rate constant
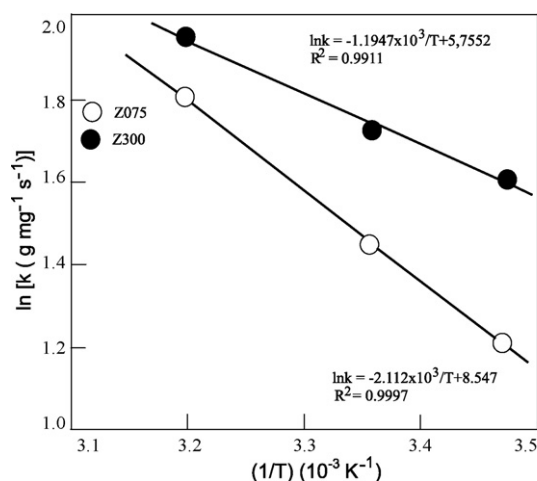


**Fig. 7.** The second-order kinetic plots for adsorption of RBBR onto Z075.



**Fig. 9.** The Arrhenius plots for the adsorption of RBBR onto Z075 and Z300.

**Table 5**
Thermodynamic parameters for the adsorption of RBBR onto different ZnO fine powder ($C_0$ = 1000 ppm, 150 rpm, pH 4.0, $m$ = 0.2 g).

| $T$ (K) | $K$ (g mol$^{-1}$ s$^{-1}$) | $K^{\#} \times 10^{-13}$ (g mol$^{-1}$) | $\Delta H^{\#}$ (J mol$^{-1}$) | $\Delta G^{\#}$ (J mol$^{-1}$) | $\Delta S^{\#}$ (J mol$^{-1}$ K$^{-1}$) |
|---|---|---|---|---|---|
| **Z075** | | | | | |
| 288.15 | 3.394 | 5.654 | 12,768 | 67,600 | −190.3 |
| 298.15 | 4.292 | 6.910 | 12,601 | 69,409 | −190.5 |
| 313.15 | 6.088 | 9.332 | 12,352 | 72,118 | −190.9 |
| **Z300** | | | | | |
| 288.15 | 5.054 | 7.747 | 5141.3 | 66,807 | −214.0 |
| 298.15 | 5.641 | 9.080 | 4975.1 | 68,732 | −213.8 |
| 313.15 | 7.017 | 11.690 | 4725.6 | 71,532 | −213.3 |

is expressed in the following form:

$$k = (5.151 \times 10^3 \text{ g mol}^{-1}\text{ s}^{-1}) \exp\frac{(-17,559 \text{ J mol}^{-1})}{RT} \tag{20}$$

$$k = (3158 \times 10^2 \text{ g mol}^{-1}\text{ s}^{-1}) \exp\frac{(-9932.7 \text{ J mol}^{-1})}{RT} \tag{21}$$

The magnitude of the activated energy $E^{\#}$ may provide a clue to the type of adsorption, physical or chemical [47], that is taking place. The activation energy for physical adsorption is usually no more than 4200 J mol$^{-1}$. The $E^{\#}$ values, calculated from the plot, were found to be 17,559 and 9932.7 J mol$^{-1}$ for the adsorption of RBBR onto Z075 and Z300, respectively. These values are of the same magnitude as the activation energy of chemical adsorption. The positive values of $E^{\#}$ indicate the endothermic nature of the adsorption process.

The Gibbs free energy for activation value, which is given in Table 5, was calculated from Eq. (18). As seen in Table 5, the positive $\Delta G^{\#}$ values indicate that the instability activation complex of the adsorption reaction increases with increasing temperature. The $\Delta H^{\#}$ values decrease positively with increasing temperature. Also, the positive $\Delta H^{\#}$ indicates, the endothermic nature of adsorption at 15–40 °C. The adsorption process in the solid–liquid system is a combination of two processes: (a) the desorption of the molecules of water (solvent) previously adsorbed and (b) the adsorption of adsorbate species [41,50,51]. The values of the negative activation entropy $\Delta S^{\#}$ confirm the decreased randomness at the solid–solution interface during adsorption.

## 4. Conclusion

Zinc oxide fine powders were prepared by homogeneous precipitation in aqueous solution with excess urea and 0.075 and 0.300 M Zn$^{2+}$ (Z075 and Z300). The ability of Z075 and Z300 to remove RBBR dye was examined, including equilibrium, kinetic and thermodynamic studies of adsorption. Experiments were performed as a function of initial pH, temperature and time. The pH of the solution played a significant role in the adsorption capacity of ZnO powder. Z075 and Z300 have high adsorption yields for dye removal from solutions at pH 4.0. The adsorption capacity of the adsorbate increased from 15 to 40 °C. The maximum dye uptake was observed at the initial dye concentration (1000 ppm). The Langmuir, Temkin, and Dubinin–Radushkevich adsorption models were used for the mathematical explanations of the adsorption equilibrium of RBBR. The $R^2$ values indicated that the adsorption of dye onto ZnO powder fit the Langmuir and Dubinin–Radushkevich isotherm models. The adsorption capacities of Z075 and Z300 for the dye were 38.9 (Langmuir); 30.2 (D–R) and 89.3 (Langmuir); 46.1 (D–R) mg g$^{-1}$, respectively. The Lagergren first-order, Ritchie second-order kinetic and intra-particle diffusion models were used to model the adsorption of the dye onto ZnO powder. It was determined that the interactions could best explained on the basis of the second-order kinetic model. The kinetic studies at the initial dye

concentration showed that the greatest adsorption capacity was achieved in 360 min for both Z075 and Z300.

The activation energies of RBBR dye over Z075 and Z300 were calculated as 17,559 and 9932.7 J mol$^{-1}$, respectively. The positive values of $E^{\#}$ indicate that the adsorption process is an endothermic process of a chemical nature. The above results confirmed the potential of ZnO fine powders as an adsorbent for basic dyes as well as other adsorbate. Overall, ZnO fine powders can be successfully used as adsorbents for color removal from aqueous solution.

## References

[1] L.M. Levinson, H.R. Philipp, ZnO varistors—a review, J. Am. Ceram. Soc. Bull. 65 (1986) 639–646.
[2] S.M. Haile, D.W. Johnson Jr., G.H. Wiseman, H.K. Boven, Aqueous precipitation of spherical zinc oxide powders for varistor applications, J. Am. Ceram. Soc. Bull. 72 (1989) 2004–2008.
[3] T.A. Gupta, Application of zinc oxide varistors, J. Am. Ceram. Soc. Bull. 73 (1990) 1817–1840.
[4] J.D. Russel, D.C. Halls, C. Leach, Grain boundary SEM conductive mode contrast effects in additive free zinc oxide, Acta Mater. 44 (1996) 2431–2436.
[5] D.R. Clarke, Varistor ceramics, J. Am. Ceram. Soc. Bull. 82 (1999) 485–502.
[6] L. Gao, Q. Li, W. Luan, Preparation and electric properties of dense nanocrystalline zinc oxide ceramics, J. Am. Ceram. Soc. Bull. 85 (2002) 1016–1018.
[7] N. Manzoor, D.K. Kim, Synthesis and enhancement of ultraviolet emission by post-thermal treatment of unique zinc oxide comb-shaped dendritic nanostructures, Scripta Mater. 54 (2006) 807–811.
[8] D.W. Johnson Jr., Nonconventional powder preparation techniques, J. Am. Ceram. Soc. Bull. 60 (1981) 221–224.
[9] T.-Q. Liu, O. Sakurai, N. Mızutani, M. Kato, Preparation of spherical fine ZnO particles by the spray pyrolysis method using ultrasonic atomization techniques, J. Mater. Sci. 21 (1986) 3698–3703.
[10] Y. Sarıkaya, M. Akınç, Preparation of alumina microshells by the emulsion evaporation technique, Ceram. Int. 14 (1988) 239–244.
[11] C.-H. Lu, C.-H. Yeh, Emulsion precipitation of submicron zinc oxide powder, Mater. Lett. 33 (1997) 129–132.
[12] S. Park, J.C. Lee, D.W. Lee, J.H. Lee, Photocatalytic ZnO nanopowders prepared by solution combustion method for noble metal recovery, J. Mater. Sci. 38 (2003) 4493–4497.
[13] Z.W. Marinković, O. Milošević, M.V. Nikolić, M.G. Kakazoy, M.V. Karpec, T.V. Tomila, M.M. Ristić, Evolution of the microstructure of disperse ZnO powders obtained by the freeze-drying method, Mater. Sci. Eng. A 375–377 (2004) 620–624.
[14] H. Li, J. Wang, H. Liu, H. Zhang, X. Li, Zinc oxide films prepared by sol–gel method, J. Cryst. Growth 275 (2005) 943–946.
[15] I. Sevinç, Y. Sarıkaya, M. Akınç, Adsorption characteristics of alumina powders produced by emulsion evaporation, Ceram. Int. 17 (1991) 1–4.
[16] M. Andrés-Vergés, M. Martinez–Gallego, Spherical and rod-like zinc oxide microcrystals: morphological characterization and microstructural evolution with temperature, J. Mater. Sci. 27 (1992) 3756–3762.
[17] L. Wang, M. Muhammed, Synthesis of zinc oxide nanoparticles with controlled morphology, J. Mater. Chem. 9 (1999) 2871–2878.
[18] C.H. Lu, C.H. Yeh, Influence of hydrothermal conditions on the morphology and particle size of zinc oxide powder, Ceram. Int. 26 (2000) 351–357.
[19] Y. Sarıkaya, I. Sevinç, M. Akınç, The effect of calcination temperature on some of the adsorptive properties of fine alumina powders obtained by emulsion evaporation technique, Powder Technol. 116 (2001) 109–114.

[20] Y. Sarıkaya, T. Alemdaroğlu, M. Önal, Determination of the shape, size and porosity of fine a-Al$_2$O$_3$ powders prepared by emulsion evaporation, J. Eur. Ceram. Soc. 22 (2002) 305–309.

[21] K. Ada, Y. Sarıkaya, T. Alemdaroğlu, M. Önal, Thermal behaviour of alumina precursor obtained by the aluminium sulphate–urea reaction in boiling aqueous solution, Ceram. Int. 29 (2003) 513–518.

[22] D. Chen, X. Jilo, G. Cheng, Hydrothermal synthesis of zinc oxide powders with different morphologies, Solid State Commun. 113 (2000) 363–366.

[23] Y. Lui, J. Dong, P.J. Hesketh, M. Liu, Synthesis and gas sensing properties of ZnO single crystal flakes, J. Mater. Chem. 15 (2005) 2316–2320.

[24] G. Palmieri, G. Cennamo, G. Sannia, Remazol Brilliant Blue R decolourisation by the fungus *Pleurotus ostreatus* and its oxidative enzymatic system, Enzyme Microb. Technol. 36 (2005) 17–24.

[25] H. Zollinger, Colour Chemistry—Syntheses, Properties and Application of Organic Dyes and Pigments, VCH Publishers, New York, 1987.

[26] V.M. Correia, T. Stephenson, S.J. Judd, Characterization of textile wastewaters, a review, Environ. Technol. 15 (1994) 917–919.

[27] G.B. Michaels, D.L. Lewis, Sorption and toxicity of azo and triphenyl methane dyes to aquatic microbial population, Environ. Toxicol. Chem. 4 (1985) 45–50.

[28] T. Robinson, G. McMullan, R. Marchant, P. Nigam, Remediation of dyes in textile effluent, a critical review on current treatment technologies with a proposed alternative, Bioresour. Technol. 77 (2001) 247–255.

[29] Y. Sarikaya, K. Ada, M. Onal, Application of the zero-order reaction rate model and transition state theory on the intra-particle sintering of an alumina powder by using surface area measurements, J. Alloy Compd. 432 (2007) 194–199.

[30] D. Ahn, W. Chang, T. Yoon, Dyestuff wastewater treatment using chemical oxidation, physical adsorption and fixed bed biofilm process, Process. Biochem. 34 (1999) 429–439.

[31] I. Langmuir, The adsorption gases on plane surfaces of glass, mica and platinum, J. Am. Chem. Soc. 40 (1918) 1361–1368.

[32] Z. Aksu, I.A. Isiloglu, Use of dried sugar beet pulp for binary biosorption of Gemazol Turquoise Blue-G reactive dye and copper (II) ions: equilibrium modeling, Chem. Eng. J. 127 (2007) 177–188.

[33] K. Vijayaraghavan, Y.S. Yun, Biosorption of C.I. Reactive Black 5 from aqueous solution using acid-treated biomass of brown seaweed *Laminaria* sp., Dyes Pigments 76 (2008) 726–732.

[34] Z. Al-Qodah, W.K. Lafi, Z. Al-Anber, M. Al-Shannag, A. Harahsheh, Adsorption of methylene blue by acid and heat treated diatomaceous silica, Desalination 217 (2007) 212–224.

[35] M.J. Horsfall, A.I. Spiff, Equilibrium sorption study of Al$^{3+}$, Co$^{2+}$ and Ag$^{+}$ in aqueous solutions by fluted pumpkin (*Telfairia occidentalis* HOOK f) waste biomass, Acta Chem. Slov. 52 (2005) 174–181.

[36] O. Abdelwahab, Evaluation of the use of loofa activated carbons as potential adsorbents for aqueous solutions containing dye, Desalination 222 (2008) 357–367.

[37] G.G. Stavropoulos, A.A. Zabaniotou, Production and characterization of activated carbons from olive-seed waste residue, Micropor. Mesopor. Mater. 82 (2005) 79–85.

[38] R. Patel, S. Suresh, Kinetic and equilibrium studies on the biosorption of reactive black 5 dye by *Aspergillus foetidus*, Bioresour. Technol. 99 (2008) 51–58.

[39] Z. Aksu, S.S. Cagatay, Investigation of biosorption of Gemazol Turquise Blue-G reactive dye by dried *Rhizopus arrhizus* in batch and continuous systems, Sep. Purif. Technol. 48 (2006) 24–35.

[40] C.W. Cheung, J.F. Porter, G. McKay, Elovich equation and modified second-order equation for sorption of cadmium ions onto bone char, J. Chem. Technol. Biotechnol. 75 (2000) 963–970.

[41] K.J. Laidler, J.H. Meiser, Physical Chemistry, The Benjamin/Cummings Publishing Company, Inc., Mento Park, CA, 1982.

[42] Y. Al-degs, M.A.M. Khraisheh, S.J. Allen, M.N. Ahmad, Effect of carbon surface chemistry on the removal of reactive dyes from textile effluent, Water Res. 34 (2000) 927–935.

[43] K. Ada, M. Gokgoz, M. Onal, Y. Sarikaya, Preparation and characterization of a ZnO powder with the hexagonal plate particle, Powder Technol. 181 (2008) 285–291.

[44] A. Demirci, E. Alver, K. Ada, M. Ozcimder, Liquid chromatographic column performance of α-alumina prepared by the reaction between aluminium sulphate and urea in boiling aqueous solution and an application to the separation of some common anions, Bull. Pure Appl. Sci. C 23 (2004) 21–37.

[46] N. Dizge, C. Aydiner, E. Demirbas, M. Kobya, S. Kara, Adsorption of reactive dyes from aqueous solutions by fly ash: kinetic and equilibrium studies, J. Hazard. Mater. 150 (2008) 737–746.

[47] C. Bauer, P. Jacques, A. Kalt, Investigation of the interaction between a sulfonated azo dye-AO7/and a TiO surface, Chem. Phys. Lett. 307 (1999) 397–406.

[48] Y.J. Kwon, K.H. Kima, C.S. Limb, K.B. Shim, Characterization of ZnO nanopowders synthesized by the polymerized complex method via an organochemical route, J. Ceram. Process. Res. 3 (2002) 146–149.

[49] R. Zhang, J. Pan, E.P. Briggs, M. Thrash, L.L. Kerr, Studies on the adsorption of RuN3 dye on sheet-like nanostructured porous ZnO films, Solar Energy Mater. Solar Cells 92 (2008) 425–431.

[50] T.V.N. Padmesh, K. Vijayaraghavan, G. Sekaran, M. Velan, Biosorption of acid blue 15 using fresh water macroalga *Azolla fliculoides*: batch and column studies, Dyes Pigments 71 (2006) 77–82.

[51] V.C. Srivastava, M.M. Swamy, I.D. Mall, B. Prasad, I.M. Mishra, Adsorptive removal of phenol by bagasse fly ash and activated carbon: equilibrium kinetics and thermodynamics, Colloids Surf. A: Physicochem. Eng. Aspects 272 (2006) 89–104.